Nitric oxide mediates local activity-dependent excitatory synapse development

Irina Nikonenko[a], Alexander Nikonenko[b], Pablo Mendez[a], Tatyana V. Michurina[c,d], Grigori Enikolopov[c,d], and Dominique Muller[a,1]

[a]Department of Basic Neuroscience, Geneva Medical Center, University of Geneva, 1211 Geneva 4, Switzerland; [b]Department of Cytology, Bogomoletz Institute of Physiology, 01024 Kiev, Ukraine; [c]Cold Spring Harbor Laboratory, Cold Spring Harbor, NY 11724; and [d]Faculty of Nano, Bio, Information, and Cognitive Technologies and Sciences, Moscow Institute of Physics and Technology, Moscow 123182, Russia

Edited* by Robert C. Malenka, Stanford University School of Medicine, Stanford, CA, and approved September 25, 2013 (received for review June 25, 2013)

Learning related paradigms play an important role in shaping the development and specificity of synaptic networks, notably by regulating mechanisms of spine growth and pruning. The molecular events underlying these synaptic rearrangements remain poorly understood. Here we identify NO signaling as a key mediator of activity-dependent excitatory synapse development. We find that chronic blockade of NO production in vitro and in vivo interferes with the development of hippocampal and cortical excitatory spine synapses. The effect results from a selective loss of activity-mediated spine growth mechanisms and is associated with morphological and functional alterations of remaining synapses. These effects of NO are mediated by a cGMP cascade and can be reproduced or prevented by postsynaptic expression of vasodilator-stimulated phosphoprotein phospho-mimetic or phospho-resistant mutants. In vivo analyses show that absence of NO prevents the increase in excitatory synapse density induced by environmental enrichment and interferes with the formation of local clusters of excitatory synapses. We conclude that NO plays an important role in regulating the development of excitatory synapses by promoting local activity-dependent spine-growth mechanisms.

synaptic plasticity | spinogenesis | dendritic spines | VASP

Neuronal activity and experience critically control the development and organization of synaptic networks by regulating the mechanisms of synapse formation and elimination. Sensory experience, motor training tasks, fear-conditioning, song-learning in birds, or exposure to novel environments in rodents are associated with major structural rearrangements of connectivity (1–8). An interesting aspect of these structural rearrangements is that they are spatially organized: the new spines formed as a result of activity tend to grow in the vicinity of activated synapses and repetitive learning promotes the formation of synaptic clusters (9–11). Despite the importance of these mechanisms for the development of brain circuits, the molecular events underlying these activity-mediated structural rearrangements of connectivity remain still essentially unknown.

Here we tested whether the diffusible messenger nitric oxide (NO) could contribute to these mechanisms. NO is produced at excitatory synapses as a result of synaptic activation through the close association of its synthesizing enzyme, neuronal nitric oxide synthase (nNOS), with the postsynaptic density and NMDA receptors (12–14). NO has thus been implicated in several aspects of synaptic function and plasticity (15–18), notably as a retrograde messenger regulating presynaptic properties, such as synaptic vesicle recycling in terminals and growth and remodeling of presynaptic varicosities (19–22). At inhibitory synapses in the ventral tegmental area, NO has even heterosynaptic effects, mediating a form of GABA-mediated long-term potentiation triggered by excitatory synapse activation (23). Studies of nNOS-deficient mice further suggest an important role of NO in cognitive functions and social behavior (24–26) and recent genetic analyses have reported associations between genetic variants of nNOS and schizophrenia (27, 28), suggesting a possible developmental role of NO for brain circuit formation. Our study provides direct evidence for such a role by demonstrating that NO is required for activity-mediated synapse formation.

Results

NO Regulates Synaptic Network Development. We first examined the role of NO in regulating the development of excitatory synapses by chronically applying the NOS inhibitor L-NAME (L-nitroarginine methyl ester) to hippocampal slice cultures [200 μM applied every day for 10 d, starting from day in vitro (DIV)1]. We used a 3D electron microscopic approach to assess spine morphology and quantified synapse density by stereology. The results illustrated in Fig. 1 show that L-NAME treatment had two major effects: it significantly reduced the density of spine synapses (0.41 ± 0.02 μm^{-3} vs. 0.83 ± 0.13 μm^{-3}, $n = 3$ slices, $P < 0.05$) and modified their morphology. Remaining spines had a larger spine volume, a larger postsynaptic density (PSD) area, and more often showed complex PSD organizations (Fig. 1 and Table S1). To confirm these observations under in vivo conditions, we then treated rat pups with either saline, D-NAME (an inactive enantiomer of L-NAME) or L-NAME. For this process, rat pups were injected with 10 μL containing saline or saline with D- or L-NAME at concentrations of 30 mg/kg body weight each day between postnatal day (P) 7 and P17. The animals were then killed and the hippocampi processed for EM analyses. These experiments revealed very similar changes: the spine synapse density decreased by 35% in L-NAME– but not D-NAME–treated

Significance

The development of brain networks is regulated through plasticity and activity-dependent mechanisms that control the continuous formation and pruning of spine synapses. However, the molecular events that contribute to these aspects of structural plasticity remain unclear. By assessing synapse development and spine dynamics in the rodent hippocampus, we find that activity-dependent spine formation is mediated by a postsynaptic signaling cascade implicating NO, cGMP, and vasodilator-stimulated phosphoprotein phosphorylation. Loss of this NO signaling mechanism interferes with the development of excitatory synapses and prevents structural adaptation of hippocampal excitatory synapses to environmental enrichment. These results provide a new understanding of the role played by NO in cognitive deficits and diseases, such as schizophrenia.

Author contributions: I.N. and D.M. designed research; I.N., A.N., P.M., T.V.M., and D.M. performed research; T.V.M. and G.E. contributed new reagents/analytic tools; I.N., A.N., P.M., and D.M. analyzed data; and I.N. and D.M. wrote the paper.

The authors declare no conflict of interest.

*This Direct Submission article had a prearranged editor.

[1]To whom correspondence should be addressed. E-mail: dominique.muller@unige.ch.

This article contains supporting information online at www.pnas.org/lookup/suppl/doi:10.1073/pnas.1311927110/-/DCSupplemental.

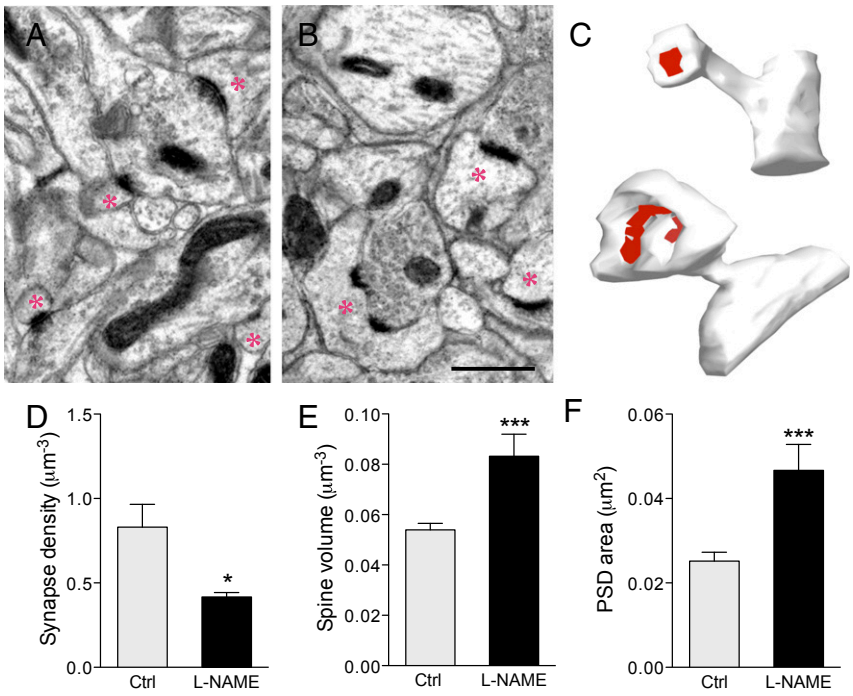

Fig. 1. Alteration of synaptic network development by chronic blockade of NO production in hippocampal organotypic slice cultures. (*A* and *B*) EM images obtained from the CA1 stratum radiatum in a control slice culture (*A*) and in a slice culture treated for 10 d with 200 μM L-NAME, a NOS antagonist. Spine synapses are marked with asterisks. (Scale bar, 0.5 μm.) (*C*) Illustration of representative 3D reconstructed spine synapses obtained from control (*Upper*, simple PSD shown in red) and L-NAME–treated slice culture (*Lower*, complex PSD shown in red). (*D*) Decrease in spine synapse density produced by chronic L-NAME treatment ($n = 3$ cultures, $P < 0.05$). (*E*) L-NAME treatment resulted in an increase in spine volume of remaining synapses (Ctrl: $n = 294$ spines, L-NAME: $n = 100$ spines, ***$P < 0.001$). (*F*) Increase in PSD area under the same conditions (***$P < 0.001$) (see also Fig. S1).

rats [L-NAME: 0.95 ± 0.05 μm^{-3} vs. D-NAME: 1.35 ± 0.04 μm^{-3} and control (Ctrl): 1.42 ± 0.06 μm^{-3}, $n = 7–14$, $P < 0.0001$]. Conversely, the spine volume and PSD area of the remaining spines increased together with the proportion of spines showing complex PSDs (Fig. S1 and Table S1). As a third approach to assess the role of NO in the development of synaptic networks, we analyzed nNOS knockout mice (nNOS-KO) (29). Fig. 2 shows 3D reconstructions of two dendritic segments obtained from nNOS-KO and WT mice perfusion-fixed at P24. As illustrated, both the number of spine synapses and the size of spines and PSDs were clearly different between nNOS-KO and WT tissue. The difference in spine synapse density was already present at P10 (0.16 ± 0.02 μm^{-3} vs. 0.34 ± 0.04 μm^{-3}, $n = 7$, $P < 0.05$); it became very significant at P15 and P24 (Table S1) ($P < 0.001$) and a small difference persisted in adult mice at P41 (Fig. 2*C* and Table S1). These changes were again correlated with an increase in spine size, in PSD area, and in PSDs with complex shapes (Fig. 2 *E* and *F*, and Table S1). Note that this decrease in spine synapse density was not compensated by shaft synapses which remained a very low fraction of total synapses (Fig. 2*C*). In addition, consistent with this decrease in synapse density, the density of presynaptic boutons was reduced (Fig. 2*G*) (2.62 ± 0.09, WT, $n = 12$ vs. 2.00 ± 0.15, nNOS-KO, $n = 10$, $P < 0.001$) and, conversely, the size of the remaining presynaptic terminals, measured as the maximal diameter in the stack, was increased (Fig. 2*H*) (0.352 ± 0.007 vs. 0.300 ± 0.007; $n = 201$ and 202; $P < 0.001$).

The changes in synapse density were not associated with detectable changes in the organization of the dendritic arborization. Measuring the fractional area occupied by dendritic profiles in EM fields randomly chosen in the CA1 stratum radiatum showed no differences between WT and nNOS-KO mice (Fig. S2 *A–C*) (2,121 and 2,185 μm^2 analyzed). Furthermore, a Sholl analysis of CA1 pyramidal neurons reconstructed from control and L-NAME–treated slice cultures showed no significant differences in the total length of apical arborizations nor in the length and distribution of dendritic segments as a function of the distance from the soma (Fig. S2 *D–F*) (total length: Ctrl: 3,132 ± 224 μm; L-NAME: 2,893 ± 208 μm; $P = 0.24$). These results therefore strongly support the idea that the loss of NO resulted in a general decrease in the number of excitatory synapses per neuron, and thus in a hypo-connectivity phenotype. Furthermore, these effects of NO blockade were not restricted to the hippocampus. In nNOS-KO mice, layer 5 of the cingulate cortex, a cortical region often implicated in schizophrenia pathology, showed the same alterations of spine density and morphology, indicating a more global implication of NO in cortical spinogenesis (Fig. 2*D*) (0.95 ± 0.04 spines/μm^3, $n = 11$ vs. 1.56 ± 0.05 spines/μm^3, $n = 10$, $P < 0.001$).

At the functional level, these structural alterations in synapse number and morphology resulted in detectable changes in excitatory transmission and intrinsic cell properties. In comparison with control slices, slice cultures chronically treated with L-NAME showed significantly enlarged miniature excitatory current amplitude, consistent with the increase in size of the remaining spine synapses (13.1 ± 0.4 pA vs. 11.3 ± 0.4 pA, $n = 23$ and 19; $P < 0.05$) (Fig. 3*C*). However, miniature current frequency was not significantly reduced (Fig. 3*D*) ($P = 0.22$) and their kinetics was not altered (rise time: 2.1 ± 0.07 ms vs. 2.2 ± 0.05 ms; half-width time: 14.0 ± 3.5 ms vs. 15.6+2.2 ms). Additionally we found no significant changes in input/output curves, facilitation ratio (Fig. S3 *A* and *B*), or AMPA/NMDA ratio (Fig. 3 *D* and *E*), suggesting preserved basal transmission properties. Analysis of intrinsic properties of CA1 pyramidal neurons further showed a slightly depolarized resting membrane potential (−56.1 ± 1.4 mV vs. −60.6 ± 1.3 mV, $n = 11–13$; $P < 0.05$), but a very significant increase in

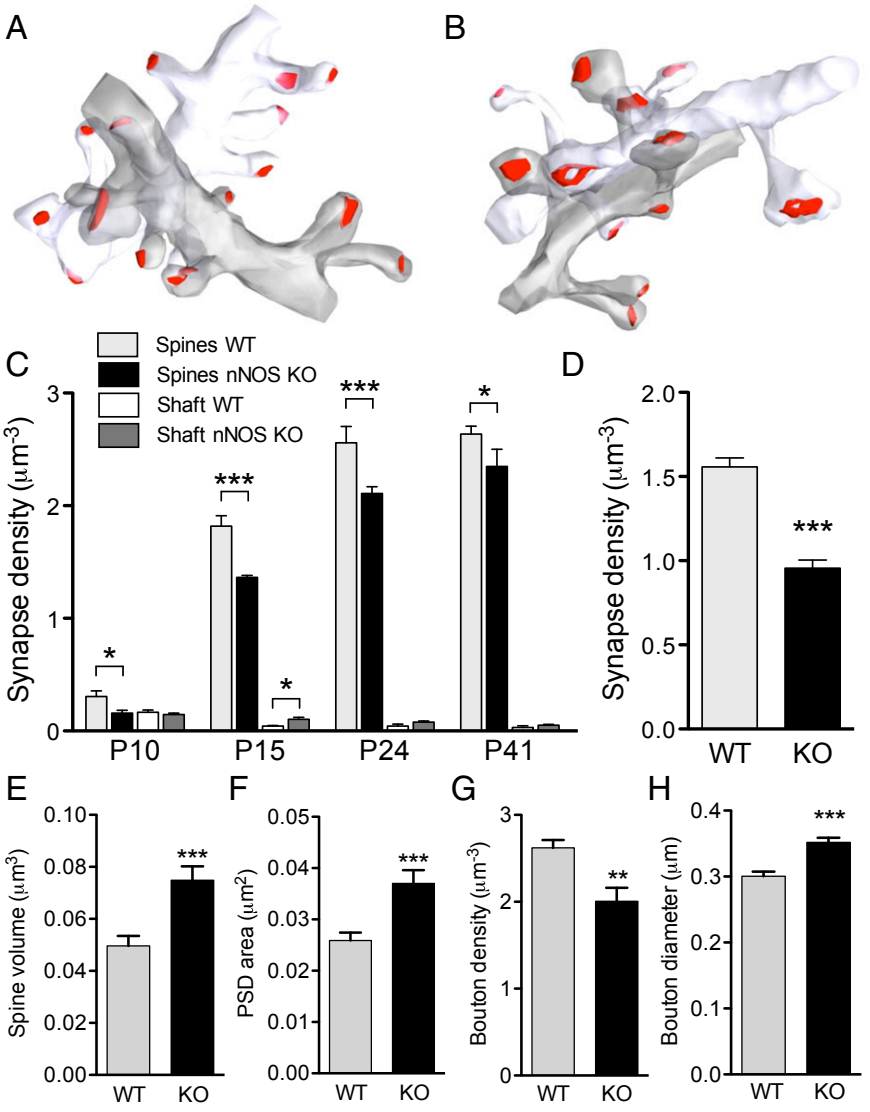

Fig. 2. Alterations of excitatory synapses development in nNOS-KO mice. (*A*) Illustration of two dendritic segments 3D reconstructed from EM serial sections of the CA1 stratum radiatum of a WT mouse (P24). (*B*) A 3D reconstruction of two dendritic segments from a nNOS-KO mouse (P24). Note the larger spine heads and PSD areas (red). (*C*) Changes in spine and shaft synapse density expressed per unit volume and observed during development in the hippocampus of nNOS-KO and WT mice. Note that the decrease in spine synapse density is not compensated by shaft synapses. (*D*) Decrease in spine synapse density in the cingulate cortex of P24 nNOS-KO mice (black bar) vs. WT mice. (*E*) Increase in the volume of spines in the hippocampal CA1 stratum radiatum of nNOS-KO vs. WT mice (P24). (*F*) Increase in PSD area of spine synapses under the same conditions. (*G*) Decrease in the density of presynaptic boutons under the same conditions. (*H*) Increase in the size of presynaptic boutons under the same conditions (black bars refer to nNOS-KO mice and gray bars to WT mice; $***P < 0.001$, $**P < 0.01$, $*P < 0.05$; quantitative data are in Table S1).

input resistance (156 ± 5.4 vs. 128 ± 7.5 MOhm; $n = 11–13$; $P < 0.01$) and a preserved excitability to depolarizing current steps applied under conditions of excitatory and inhibitory transmission blockade (Fig. S3 *C–E*). Taken together, these results suggest some adaptative mechanisms to chronic blockade of NO production and are consistent with the existence of a hypo-connected synaptic network, but containing more efficient synapses.

NO Controls Basal and Activity-Mediated Spine Growth. To understand the mechanisms underlying the decrease in synapse density, we investigated how NO affected spine dynamics in mRFP-transfected CA1 hippocampal neurons in slice cultures using a repetitive imaging approach. Under basal conditions, a fraction of spines is formed and eliminated every day (22.9 ± 1.7% and 17.0 ± 1.9%, $n = 27$) (Table S2), maintaining a relatively stable number of synaptic contacts. When slice cultures were treated with the NOS inhibitor L-NAME for 24 h (200 μM), the fraction of newly formed spines decreased by 75% to 5.6 ± 1.1% ($n = 16$, $P < 0.001$), but the rate of spine elimination was not modified (18.7 ± 1.8%, $n = 16$) (Fig. 4 *A*, *C*, and *D*). As a result, spine density decreased by about 20% within 24 h (from 1.06 ± 0.02 μm^{-1} to 0.86 ± 0.02 μm^{-1}, $n = 27$ and 16; $P < 0.001$) (Fig. 4*E*). These effects were initiated quite rapidly, as analyses carried out only 5 h after L-NAME treatment already indicated a very significant decrease in spine growth mechanisms (new spines formed at 5 h: Ctrl: 9.5 ± 1.8% vs. L-NAME: 0.7 ± 0.4%, $n = 6$; $P < 0.001$). To further analyze this mechanism, we treated slice cultures for 24 h with 2 mM 8-Br-cGMP (cGMP), a stable cell-permeable analog of cGMP, which often contributes to NO signaling. As shown in Fig. 4, cGMP produced the converse effect of L-NAME and greatly enhanced spine formation without affecting spine loss (Fig. 4 and Table S2) ($n = 8$, $P < 0.05$). Note

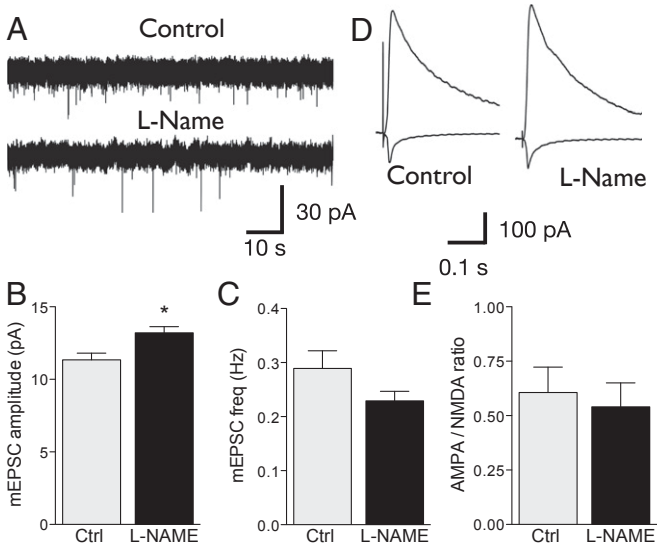

Fig. 3. Alterations of synaptic transmission in L-NAME treated hippocampal slice cultures. (*A*) Illustration of mEPSCs recorded in CA1 pyramidal neurons of control hippocampal slice cultures and slice cultures treated with L-NAME (200 μM) between DIV1 and DIV10. (*B*) Increase in mEPSC amplitude in slice cultures chronically treated with L-NAME vs. control slices (n = 21 and 18; *P < 0.05). (*C*) mEPSC frequency under the same conditions (n = 21 and 18; P = 0.22). (*D*) Illustration of AMPA/NMDA currents recorded at −70 mV and +40 mV in CA1 pyramidal neurons of control and L-NAME treated slice cultures. (*E*) Absence of modifications of the AMPA/NMDA ratio under the same conditions.

that L-NAME no longer blocked spine formation when slice cultures were treated with cGMP, indicating that cGMP acted downstream of NO production (n = 8). Finally, blockade of cGMP-dependent protein kinase with Rp-8-cGMP (100 μM) applied for 24 h reproduced the effects of L-NAME, thus confirming that NO acted through a cGMP signaling cascade (n = 8, P < 0.001) (Table S1).

As spine turnover is regulated by neuronal activity, we then tested whether the effect of NO was also activity-dependent. As shown in Fig. 4*F*, blockade of neuronal and synaptic activity with tetrodotoxin (TTX, 1 μm) or D-AP5 (50 μM) for 24 h markedly reduced spine growth without affecting spine elimination, thus reproducing the effects of L-NAME (Fig. 4*F* and Table S2) (n = 10 and 6, P < 0.01). Addition of L-NAME to TTX did not further block spine growth (n = 8, P < 0.01), but the effect of TTX could be reversed through a concomitant application of cGMP, indicating that cGMP could reverse the effects of activity blockade (n = 9, P < 0.01). Conversely, application of θ-burst stimulation (TBS) to slice cultures greatly enhanced spine turnover over the next 24 h, resulting both in an increased formation and increased elimination of spines (Fig. 4*F* and Table S2) (n = 11, P < 0.001). This increase in spine growth was again fully blocked by L-NAME (n = 7, P < 0.001), but spine elimination remained unchanged. The increased spine formation triggered by TBS was previously found to preferentially occur in close proximity to activated synapses (9). We therefore tested whether this local spine growth triggered by TBS still occurred in the presence of L-NAME (Fig. 4 *G* and *H*). For this process, we assessed the probability for a new spine to grow less than 1 μm apart from a preexisting one. To allow comparisons, we selected dendritic segments of comparable densities for these experiments (density: 1.11 ± 0.08 μm^{-1} for control and 1.18 ± 0.09 μm^{-1} for L-NAME). We compared three conditions: basal turnover under control conditions, spine growth induced by TBS under control conditions, and spine growth induced by TBS in the presence of L-NAME. Under basal conditions, the probability of a newly formed spines to grow close to a previously existing one was 0.53 ± 0.01 (Fig. 4*H*) (n = 57 spines, 11 cells). Applying TBS to Schaffer collaterals resulted in an increased spine growth over the next 24 h and these newly formed spines showed a clear tendency to appear close to preexisting spines (Fig. 4*G*) (probability: 0.76 ± 0.02, n = 67 spines, 6 cells, P < 0.01). In contrast, application of TBS in the presence of L-NAME resulted in a reduced number of new spines and these spines showed no preferential growth close to an existing spine (probability: 0.46 ± 0.07, n = 15 spines, 7 cells).

Effects of NO Are Mediated by the Phosphorylation of Postsynaptic Vasodilator-Stimulated Phosphoprotein. To identify the mechanism and site of action (pre- or postsynaptic) of NO, we focused on possible downstream targets of cGMP-dependent protein kinase (PKG), such as vasodilator-stimulated phosphoprotein (VASP), a member of the Ena/VASP family, involved in the regulation of the cytoskeleton and elongation of actin filaments (30–32). Notably VASP can be phosphorylated at two main sites, Ser^{157} and Ser^{239} by PKG. Phosphorylation of these sites has been shown to be important for the regulation of the cytoskeleton by VASP (33). To test whether VASP phosphorylation could mediate the effects of NO on spine growth, we used a mutation approach and cotransfected hippocampal pyramidal neurons with mRFP and EGFP-tagged constructs of either WT VASP, a phospho-resistant mutant VASP (AAT-VASP), in which the two phosphorylation sites Ser^{157} and Ser^{239} have been mutated into alanine, or a phospho-mimetic mutant (DDT-VASP), in which the two phosphorylation sites have been mutated to aspartate (34). VASP is highly expressed in dendrites and in spines (Fig. S4), as indicated by transfections of EGFP-VASP. Furthermore, activation of slice cultures with carbachol (10 μM, 1 h), a cholinergic agonist that promotes rhythmic activity, leads to a significant increase in the level of VASP phosphorylation that may last several hours after treatment (Fig. S4). Analysis of spine dynamics in cells transfected with the different VASP mutants showed that expression of WT VASP or of the phospho-mimetic VASP mutant markedly enhanced spine growth mechanisms, reproducing the effect of TBS or 8-Br-cGMP (Fig. 5 and Table S2) (n = 9, P < 0.001 and n = 9; P < 0.01). Note that L-NAME became ineffective in blocking spine growth when the phospho-mimetic mutant was expressed in pyramidal neurons (n = 8, P < 0.01), indicating that DDT-VASP acts downstream of NO and that the regulation of spine growth is postsynaptic (Fig. 5*D*). In contrast, expression of the phospho-resistant VASP mutant reproduced the effects of L-NAME and strongly blocked spine growth mechanisms (n = 11, P < 0.001). Note that spine growth was strongly inhibited by the phospho-resistant mutant even in the presence 8-Br-cGMP (n = 11, P < 0.001), confirming the importance of VASP as a downstream postsynaptic target of PKG. In addition, VASP phospho-mutants only affected spine growth mechanisms and not spine elimination, as it is the case for L-NAME or cGMP (Table S2).

We then examined further whether VASP phosphorylation also contributed to the changes in spine growth mediated by synaptic activity. For this process we applied TBS to neurons transfected with either WT VASP or the phospho-resistant mutant VASP-AAT. As shown in Fig. 5*E*, TBS-mediated spine growth was fully blocked in AAT-VASP transfected cells (Table S2) (n = 6, P < 0.001), whereas overexpression of WT VASP was sufficient to reproduce the effects of TBS and no further increase could be observed (n = 9, P < 0.05). Taken together, these results suggest that postsynaptic VASP phosphorylation is sufficient and necessary for activity-mediated spine growth.

NO Is Required for Enrichment-Induced Structural Plasticity and Excitatory Synapse Clustering. We then wondered whether the role of NO in regulating local spine growth could be implicated in learning mechanisms under in vivo conditions. For this hypothesis,

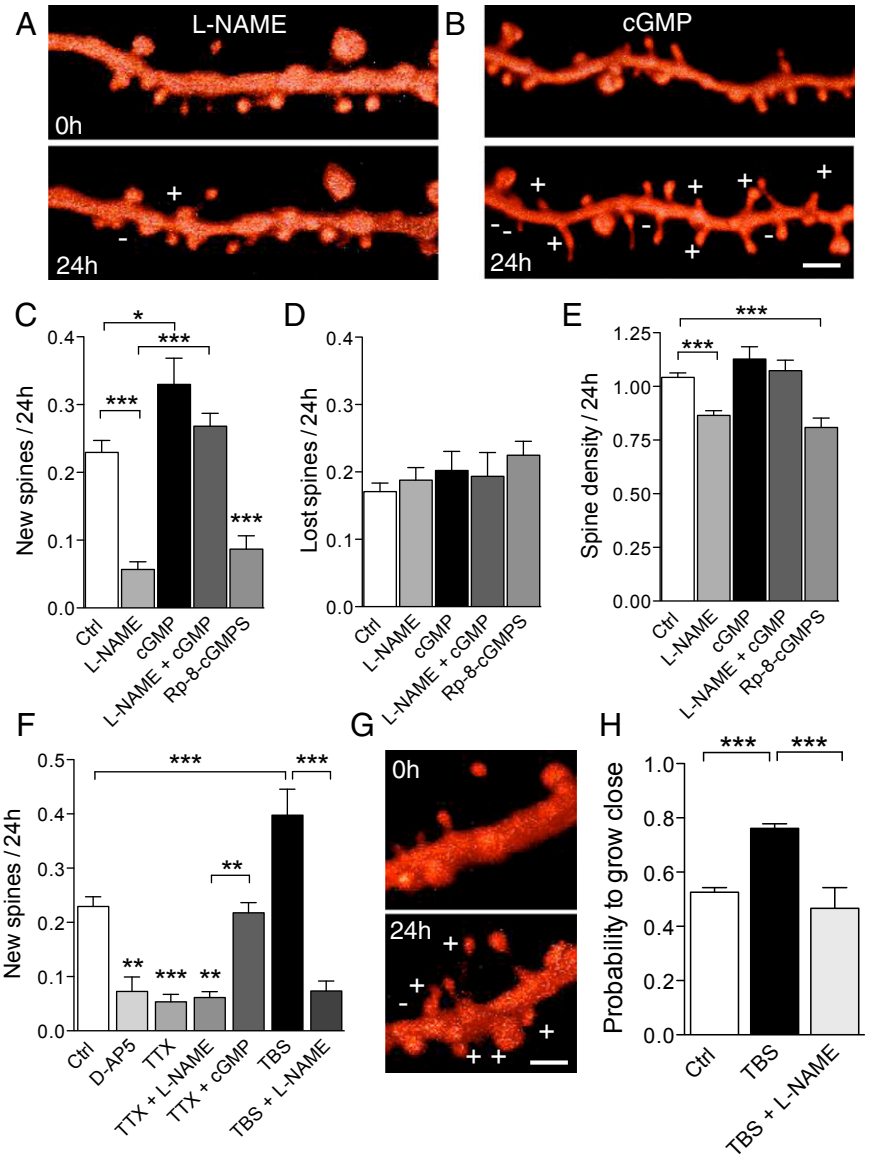

Fig. 4. Regulation of local, activity-dependent spine growth by NO. (*A*) Illustration of spine turnover over a period of 24 h in a transfected CA1 pyramidal neuron treated with L-NAME. (*B*) Same but in a pyramidal neuron exposed to 2 mM 8-Br-cGMP (cGMP) for 24 h. (Scale bar, 0.5 μm.) (*C*) Quantitative analyses of new spine formation over periods of 24 h in control conditions ($n = 27$), slice cultures treated for 24 h with L-NAME ($n = 16$), slice cultures treated for 24 h with cGMP ($n = 8$), slices cultures treated with L-NAME together with cGMP ($n = 8$), and slice cultures treated with Rp-8-cGMPS ($n = 8$). Note that cGMP reverses the effect of L-NAME, indicating that it acts downstream of NO. (*D*) L-NAME, cGMP and Rp-8-cGMPS do not affect mechanisms of spine elimination over 24 h. (*E*) Resulting changes in spine density over 24-h periods under the same conditions. (*F*) NO modulation of new spine formation is activity-dependent. D-AP5 (50 μM; $n = 6$) and TTX (1 μM, $n = 10$) reproduce the effect of L-NAME treatment ($n = 16$), the effects of TTX and L-NAME are not additive ($n = 8$) and cGMP reverses the block by TTX ($n = 9$). TBS enhances spine formation mechanisms ($n = 11$) and this effect is blocked by L-NAME ($n = 7$). (*G*) Illustration of the effect of TBS on a clustered growth of new spines. (Scale bar, 1 μm.) (*H*) Probability for a newly formed spine to grow less than 1-μm apart from another preexisting spine under control conditions ($n = 57$ spines analyzed), 24 h following TBS ($n = 67$, $P < 0.001$, ANOVA) and 24 h following TBS applied in the presence of L-NAME ($n = 15$) (see Table S2 for quantitative data). $^{*}P < 0.05$, $^{**}P < 0.01$, $^{***}P < 0.001$.

we tested whether the synaptic rearrangements promoted by experience, such as environmental enrichment, could be affected by a deficit in NO. Previous work by different laboratories has shown that exposure of mice to environmental enrichment results in a significant and detectable increase in spine density (35–37). We therefore tested whether these synaptic network adaptations were still functional in NO-deficient mice. Young mice (WT and nNOS-KO; P14) were either exposed for 10 d to an enriched environment (EE) or maintained under conventional housing conditions. We then proceeded to a morphological analysis of synapse density at the EM level using a stereological approach. As shown in Fig. 6, exposure of WT mice to EE for 10 d resulted in a significant increase in spine density (WT-EE: 9.2 ± 0.2 μm^{-3}, $n = 10$ vs. WT: 7.9 ± 0.3 μm^{-3}, $n = 13$, $P < 0.01$). In contrast, in nNOS-KO mice, this effect was fully blocked and the spine density remained significantly lower than in WT mice (KO: 6.2 ± 0.1 μm^{-3}, $n = 11$ vs. KO-EE: 6.5 ± 0.1 μm^{-3}, $n = 10$).

While we were analyzing the 3D distribution of synapses in the tissue, we were struck by the existence of small clusters of synapses with several synapses lying close to each other [i.e., at distances of 0.5–1 μm, which correspond to estimations of the diffusion distance of NO generated at synaptic sites (22)] (Fig. 7

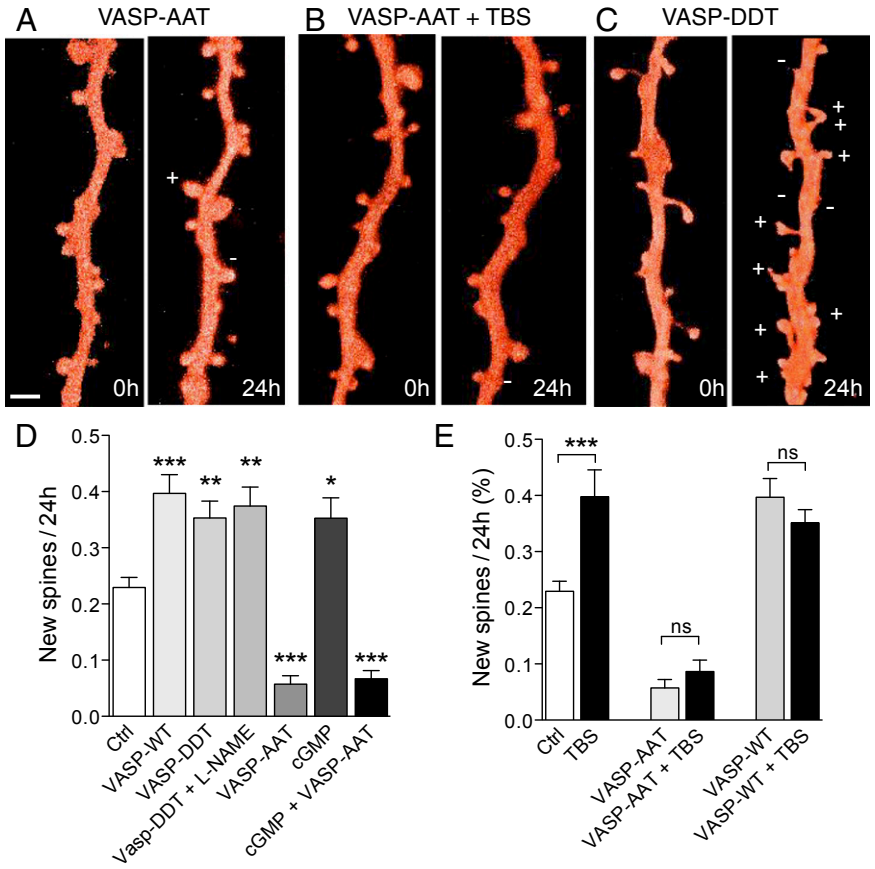

Fig. 5. VASP phosphorylation mediates NO-stimulated and activity-dependent spine growth. (*A*) Illustration of the decrease in spine formation observed in phospho-resistant VASP-AAT–transfected CA1 pyramidal neurons. (Scale bar: 1μm.) (*B*) Application of TBS no longer enhances new spine formation in VASP-AAT–transfected pyramidal neurons. (*C*) Enhanced spine formation in pyramidal neurons transfected with phospho-mimetic VASP-DDT. (*D*) Quantitative analyses of spine growth mechanisms under various conditions. Expression of both VASP-WT (n = 9) and the phospho-mimetic VASP-DDT (n = 9) enhanced spine growth mechanisms. The effect of VASP-DDT was no longer blocked by L-NAME (n = 8). In contrast, the phospho-resistant VAST-AAT reproduced the effects of L-NAME and inhibited spine growth (n = 11). Application of cGMP, which enhanced spine formation under control conditions (n = 7), was no longer effective in VASP-AAT transfected neurons (n = 11). (*E*) TBS applied to CA1 pyramidal neurons transfected with VASP-AAT no longer enhances spine growth (n = 6). Conversely, overexpression of VASP-WT reproduces and occludes the effect of TBS (n = 9) (see also Fig. S4). ns, not significant. *P < 0.05, **P < 0.01, ***P < 0.001.

A–*C*). We therefore wondered whether NO could be implicated in the formation of these synaptic clusters. For this process, we spotted the location of all excitatory synapses present in small volumes of hippocampal stratum radiatum (48 $\mu m^{-2} \times 0.36$ μm: 17.3 μm^{-3}) (Fig. 7*A*) and calculated the fraction of synapses that had a neighbor synapse at a distance less than 0.5 μm, using a minimum spanning-tree algorithm. As shown in Fig. 7*D*, a relatively high proportion of synapses have very close neighbors in WT animals (43.2 ± 3.1%, n = 13). This fraction further increases following exposure of WT mice to EE (50.6 ± 1.1%, n = 11, $P < 0.05$). In nNOS-KO mice, the proportion of synapses having a close neighbor was significantly reduced and no longer changed after EE (KO: 34.6 ± 1.4, n = 12, $P < 0.05$; KO-EE: 32.0 ± 2.4, n = 14). Because this parameter is also sensitive to variations in synapse density, we then proceeded to an analysis of the radial distribution of synapses, calculating the proportion of all synapses located within concentric circles around each synapse, a parameter that is independent of synapse density (Fig. 7 *B* and *C*). For comparison, we also calculated these values using simulated random distributions of synapses. As illustrated in Fig. 7*E*, the fraction of synapses present at short distances (i.e., at less than 0.6 μm around each synapse) was significantly higher in WT mice and in WT mice exposed to an enriched environment than in simulated random distributions. This effect was specific for synapses located at short distances because the fraction of synapses present slightly farther apart (i.e., 0.6–1 μm from each synapse) were not different from random distributions (Fig. 7*F*). This result thus confirms the existence of a synapse clustering effect in WT mice and mice exposed to EE. In contrast, in nNOS-KO mice and nNOS-KO mice exposed to EE, the distribution of synapses did not differ from random distributions at all distances analyzed, thereby indicating that NO is required for this clustering effect. Taken together, these results provide evidence that blockade of NO production not only prevents learning-mediated structural plasticity, but also affects the distribution of synapses in the tissue by interfering with synapse clustering mechanisms.

Discussion

This study uncovers an important function of NO, which is to promote activity-dependent spine formation during development, and so contribute to the selectivity of excitatory synaptic networks. Several recent in vivo studies have provided evidence that a structural reorganization of synaptic connections is directly associated with learning paradigms (8). In a series of elegant experiments analyzing cortical plasticity during and following learning of a motor dexterity task, Zuo's and Gan's laboratories demonstrated that an increase in spine formation and a selective stabilization of these new spines closely correlated with the acquisition and retention of the task (3, 4). Similar findings have

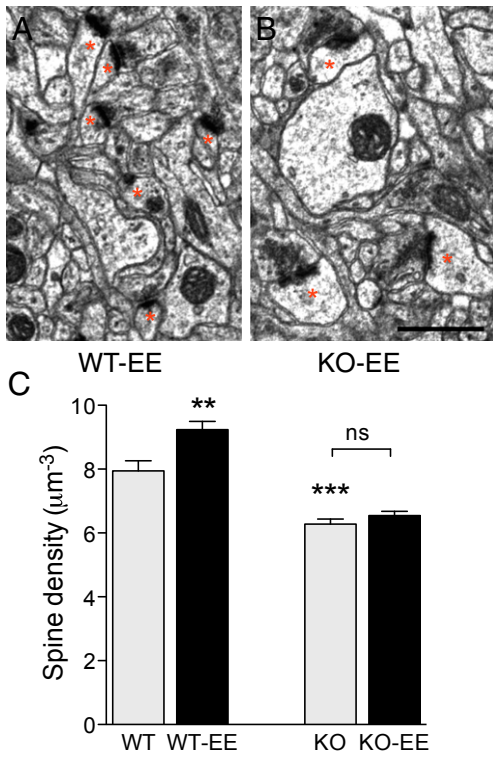

Fig. 6. Enriched environment-induced spine formation is prevented in nNOS-KO mice. (*A*) EM illustration of spine density in the CA1 stratum radiatum of a WT mouse exposed for 10 d (P14–24) to an EE. (*B*) Same but for a nNOS-KO mouse. (Scale bar, 0.5 μm.) (*C*) Increased spine density measured using a stereological approach in WT mice (n = 12 volumes analyzed, 3 mice) and WT mice exposed to an enriched environment (n = 10 volumes, 3 mice, $^{**}P < 0.01$). In nNOS-KO, the spine density is decreased (n = 11 volumes, 3 mice, $^{***}P < 0.001$) and EE no longer promotes an increase in synapse density (n = 10 volumes, 3 mice). ns, not significant.

been reported in several other experimental or behavioral paradigms (5, 7, 38, 39), and together with many other observations, these results have led to the concept that activity is a major architect of the construction of synaptic networks during development.

However, how exactly synaptic activity or experience drives synapse formation remains poorly understood. The present results support a scenario in which NO plays a major role. Activation of the synapse, through an involvement of NMDA receptors and calcium influx, could lead to the activation of nNOS, closely associated to PSD-95 in the postsynaptic density. This process would result in the release of NO and the activation of a cGMP-PKG cascade in close-by dendrites and the phosphorylation of the cytoskeletal regulatory protein VASP. As a result, active synapses would stimulate the growth of new protrusions in their vicinity, promoting the formation of clusters of synapses present at very short distances, as seen in WT mice following environment enrichment. This mechanism could be very important as it could favor the formation of synapses with particularly active partners.

Several observations support this interpretation. First, the close link between nNOS, PSD-95 and NMDA receptors is well documented (12, 13, 40). Several studies have shown that patterns of activity that trigger synaptic plasticity are able to promote NO release and that these effects can be blocked by the NOS antagonist L-NAME (15, 22, 23, 41). Second, our study provides direct evidence that interference with NO production prevents the development of spine synapses under in vitro and in vivo conditions, in the rat and mouse hippocampus, and also in the cingulate cortex. It is interesting that the decrease in synapse density produced by the loss of NO signaling was compensated by an increase in size and efficacy of remaining synapses. Somehow, this phenomenon shares similarities with the homeostatic regulations implicated in synaptic scaling (42) and, together with changes in intrinsic properties, could contribute to maintain a given level of neuronal activity. Thus, the loss of NO signaling not only affects the development of excitatory synapses, but probably also modifies the distribution of synaptic weights within the network. Third, the synaptic growth promoting effects of NO are clearly linked to synaptic activity. Blockade of activity through TTX or an NMDA receptor antagonist reproduced the effects of L-NAME, whereas L-NAME prevented the increased spine growth triggered by high frequency stimulation. Conversely, activation of the NO-cGMP signaling cascade reproduced and occluded the effects of high-frequency stimulation and its blockade prevented all effects of activity. Furthermore, the present in vivo experiments clearly show that experience-mediated spine formation is fully prevented in nNOS-KO mice, providing an additional link between neuronal activity, NO signaling, and spine growth mechanisms.

At the molecular level, the mechanisms through which NO controls spine growth appear to mainly involve a postsynaptic regulation of the actin cytoskeleton through a cGMP-PKG cascade. This finding is consistent with many other studies that have identified guanylyl cyclase and cGMP formation as a main target of NO signaling (22, 43, 44). Our data further indicate that the effect of NO on spine growth is mediated through the phosphorylation of VASP. VASP regulates actin polymerization in a phosphorylation-dependent manner and has been implicated in neurite elongation and spine formation (30–34, 45). Our results with the VASP phospho-mutants further identify VASP phosphorylation as a key mechanism for activity-dependent spine formation, providing evidence that VASP phosphorylation is both sufficient and necessary to mediate the effects of synaptic activity on spine growth. Additionally, these experiments show that the regulation of spine growth by activity is mainly operated by postsynaptic mechanisms. This finding is consistent with experiments showing that glutamate, when applied locally, can rapidly trigger the growth of new spines and the formation of synapses (46, 47). It could be argued that it is glutamate spillover that contributed to spine growth in our experiments. However, the effect of glutamate on spine formation occurred within seconds (46, 47), but the effect of activity on spine formation develops over minutes to hours when glutamate is no longer present (9). In addition, glutamate is the main trigger for the formation of NO and thus the two effects could very well be linked, with fast acting glutamate activating a longer-acting NO signaling pathway. It is also very likely that other mechanisms implicated in the regulation of the actin cytoskeleton could contribute to these effects. Recent data have, for example, implicated Rho-GTPases and PAK signaling in the control of activity-dependent spine formation (48). Another interesting aspect of NO is that, although it promotes spine growth as shown here, it can also promote the growth and differentiation of new presynaptic boutons (19, 20, 45, 49). Consistent with this finding, nNOS-KO mice also showed a major decrease in presynaptic bouton density and a correlated increase in terminal size. NO might therefore be the ideal molecule able to simultaneously act pre- and postsynaptically to promote synaptic contact formation. This dual activity-dependent growth promoting effect could be critically important during development to allow synapse formation to preferentially occur between active partners.

Taken together, these results indicate that NO produced by activated synapses can promote the growth of new spines in a small volume of around 1–1.5 μm in diameter around a synapse. This result can favor a mechanism of activity-dependent spine

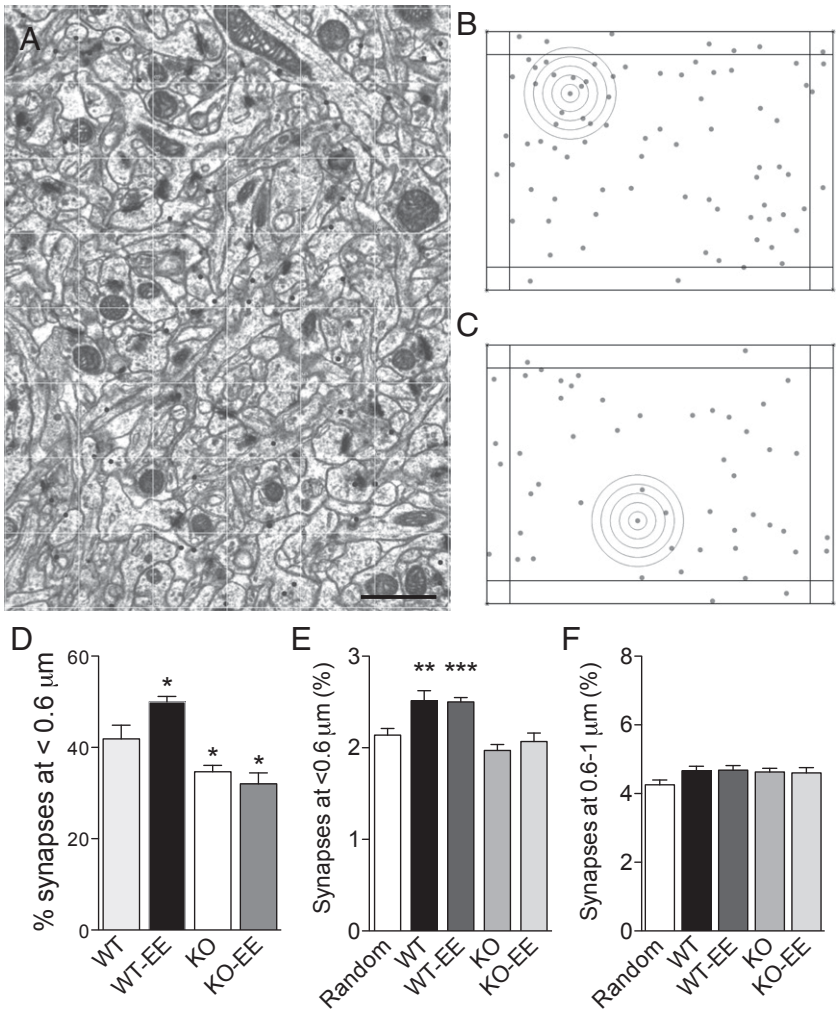

Fig. 7. Clustered distribution of synapses in WT mice but not nNOS-KO mice. (*A*) Illustration of one of the EM serial sections (from a stack of six sections, stratum radiatum, CA1 hippocampus) used for analysis of spine synapse distribution. Black points indicate the projection of the location of the center of postsynaptic density on a 2D plane. (Scale bar, 1 μm.) (*B*) Illustration of the distribution of synapses represented by gray dots in a WT mouse. The concentric circles centered on a given dot illustrate the radial analysis. (*C*) Same but in a nNOS-KO mouse. (*D*) Fraction of synapses having a close neighboring synapse within 0.5-μm distance in WT mice (P24, $n = 14$ volumes analyzed), WT mice exposed to an EE (P14–24, $n = 12$, $P < 0.05$), nNOS-KO mice (P24, $n = 12$, $P < 0.05$), and nNOS-KO mice exposed to EE (P14–24, $n = 14$, $P < 0.05$). (*E*) Proportion of spine synapses found at short distance (<0.6 μm) from each reference synapse. Data were calculated for WT mice ($n = 14$ volumes), WT mice exposed to EE (WT-EE, $n = 12$), nNOS-KO mice ($n = 12$), nNOS-KO mice exposed to EE ($n = 14$) and for simulated random distributions (Random, $n = 14$). Note the increased proportion of clustered synapses in WT, but not nNOS-KO mice (**$P < 0.01$, ***$P < 0.001$). (*F*) The proportion of spine synapses found at distances of 0.6–1 μm from each reference synapse does not differ from a random simulation.

clustering and also enhance the probability that these new synapses target active axons. NO would thus represent a critical messenger to ensure a proper development of excitatory synaptic networks through activity-related rewiring. This unique role of NO could also account for the reported association between nNOS genetic variants and schizophrenia (28). Interestingly, a recent imaging study in humans expressing a polymorphism of nNOS associated with schizophrenia shows that they exhibit gray matter volume alterations and cognitive deficits (50).

Materials and Methods

Organotypic Cultures, Constructs, and Confocal Imaging. Organotypic hippocampal slice cultures were prepared from 6- to 7-d-old rat pups, as previously described (51). To analyze the developmental effects of loss of NO, slice cultures were treated with L-NAME (200 μM for 10 d starting on DIV1). To analyze spine dynamics, the slices were transfected or cotransfected at DIV8 with different constructs using a biolistic technique (hand-held Gene Gun; DNA-coated gold microcarriers; 1.6 μm; Bio-Rad Laboratories), according to the instructions of the manufacturer. WT VASP-SST, Ser phosphorylation-resistant mutant VASP-AAT (S157A/S239A), and Ser phosphorylation-mimetic mutant VASP-DDT (S157D/S239D) were introduced in the expression vector pEGFP-C1, as previously described (34). These constructs were a generous gift of David B. Pearse (Johns Hopkins Bayview Medical Center, Baltimore, MD). Transfected fluorescent cells were used for repetitive confocal imaging experiments beginning from the fourth day after transfection, and spine turnover analysis was carried out as previously described (9). Pharmacological treatments for spine dynamics were carried out at DIV12–13. In all cases, the drugs were added to the culture medium 30 min before the first confocal observation to allow penetration into the cultures, confocal imaging was carried out in the presence of the drugs, and the drugs were maintained for the next 24 h.

Mice. The experimental protocols were reviewed and approved by the Ethics Committee of the University Medical Center of Geneva, by the Cantonal Veterinary Office, Geneva, Switzerland, and by the Cold Spring Harbor Laboratory Animal Use and Care Committee. The nNOS-null mouse mutant line KOex6 was generated by targeting the essential heme-binding site of the nNOS enzyme, leading to complete loss-of-function mutant mice (29). Neither nNOS mRNA, nor nNOS protein, nor nNOS activity was detected in these loss-of-function mutant mice.

Animals were genotyped by PCR analysis of mouse tail DNA by using two pairs of primers specific to one of each: the WT allele (5′-GGCTCATTGA-CAACTCCTGCT-3′ and 5′-ATGTGGGCCTTGGAGCCAAAC-3′, GenBank accession no. AF534820) or to the neomycin phosphotransferase gene of the *KOex6* allele (5′ -TGCCGAGAAAGTATCCATC-ATGGCTGATGC-3′ and 5′-CAGAA-GAACTCGTCAAGAAGGCGATA-GAAGG-3′). The nNOS-null mouse mutant line KOex6 was maintained at the Cold Spring Harbor Laboratory Animal care facility (Laboratory of Animal Resources) in mouse microisolator cages. $nNOS^{-/-}$ mice and their WT littermates were provided with liquid chow and diet gel with ad libitum access to water. Use of animals was reviewed and approved by the Cold Spring Harbor Laboratory Animal Use and Care Committee.

Electrophysiology. For electrophysiological recordings, organotypic slice cultures were continuously perfused (2–2.5 mL/min) with a solution containing: NaCl 124 mM, KCl 1.6 mM, $CaCl_2$ 2.5 mM, $MgCl_2$ 1.5 mM, $NaHCO_3$ 24 mM, KH_2PO_4 1.2 mM, Gabazine (SR-95531) 0.01 mM, glucose 10 mM, ascorbic acid 2 mM; saturated with 95% (vol/vol) O_2 and 5% CO_2 (pH 7.4; temperature 31 °C). TTX (1 μM) was added to the perfusion solution for spontaneous excitatory miniature recordings (mEPSC). L-NAME (200 μM) was added to the perfusion medium while recording from the cultures chronically treated with L-NAME.

In slice cultures, TBS was carried out by placing a stimulation electrode in the CA3 area and recording evoked field potentials in the CA1 area. TBS consisted of five bursts at 5 Hz with each burst composed of four pulses at 100 Hz. This pattern was applied twice at 10-s intervals and then the slices were put back in the incubator. Input-output curves were generated by recording excitatory field potentials in the stratum radiatum of slice cultures and applying stimulations of increasing intensity to a group of CA3 neurons. Facilitation was assessed by measuring the ratio of slopes of excitatory postsynaptic potentials evoked by paired stimulations of varying interpulse intervals (30, 50, 100, and 150 ms).

Whole-cell recordings were carried out using patch pipettes filled with a solution containing: 125 mM $CsMeSO_3$, 10 mM Hepes, 5 mM EGTA, 2 mM $MgCl_2$, 5 mM QX-314, and 4 mM MgATP. To induce evoked EPSCs, a metallic stimulating electrode placed in the stratum radiatum at about 300 μm from the recorded cell soma. To avoid epileptical activity, a cut was made between the CA3 and CA1 region and NBQX (0.3 μM) was added to the perfusion solution. Measurements were done at −70 and 40 mV holding potential for AMPA- and NMDA-mediated currents, respectively. Recordings were obtained using an Axopatch 200B (Molecular Devices), filtered at 2 kHz, and digitized at 5–10 kHz and stored on hard disk. Data acquisition and analysis were performed using pClamp 9.

Custom written software (Detector, courtesy J. R. Huguenard, Stanford University, Stanford, CA) was used for analyzing mEPSC events. Briefly, individual events were detected with a threshold-triggered process from a differentiated copy of the real trace. Detection criteria (threshold and duration of trigger for detection) were adjusted to ignore slow membrane fluctuations and electric noise, while allowing maximal discrimination of sEPSCs. For determining AMPA/NMDA ratios, the NMDAR-mediated component of evoked EPSCs was measured as the EPSC amplitude at +40 mV recordings at 200 ms after stimulation, when the AMPAR-mediated component has decayed back to baseline. Membrane potential, input membrane resistance and neuronal excitability were measured under whole-cell patch configuration, with excitatory and inhibitory transmission blocked by D-AP5 (50 μM), DNQX (10 μM), and Gabazine (10 μM), and with a potassium gluconate-based internal solution.

Morphology and Electron Microscopy. Slice cultures or vibratome cut slices from perfusion-fixed brains were embedded in EPON, cut for ultrathin serial sections, and collected on single-slot Formvar-coated grids according to standard procedures (20). Images of the neuropil from the middle portion of CA1 stratum radiatum or from the cingulate cortex layer V were taken at a magnification of 9,700× using a transmission electron microscope Tecnai G212 (FEI Company) equipped with digital camera (Mega View III; Soft Imaging Systems). Digital serial electron micrographs were aligned using Photoshop software (Adobe). Three-dimensional reconstructions as well as surface, volume, and length measurements were carried out using Neurolucida software (v6.02; MicroBrightField).

For serial EM, ribbons of up to 300 sections were cut in the middle portion of the apical arborization of CA1 pyramidal neurons (stratum radiatum) and collected on single-slot grids. Spine synapses were analyzed and reconstructed in randomly selected volume samples obtained in the places devoid of big processes and cell bodies. On EM images, spine synapses were distinguished by the presence of a spine head with a PSD facing a presynaptic bouton. Complex PSDs were defined by the presence of a discontinuity on a single section. Presynaptic terminals were identified by the presence of an enlargement of the axonal shaft containing synaptic vesicles and facing at least one PSD. The density of spine synapses was estimated using the physical disector method (52) on consecutive serial sections, as previously described (20). Three-dimensional illustrations were made with the software Reconstruct developed by J. C. Fiala and K. M. Harris (www.bu.edu/neural/Reconstruct.html) followed by color rendering with 3D Studio Max (Autodesk).

The dendritic arborization of CA1 pyramidal neurons in organotypic slice cultures was analyzed by taking confocal images of mRFP-transfected cells. Apical dendritic arbors were then outlined on stacks of images and analyzed using Neurolucida software. To assess the fractional area of dendritic profiles, we analyzed randomly chosen CA1 neuropil fields obtained by the alignment of four (2 × 2) overlapping electron micrographs taken at a magnification of 9,700× with a Tecnai electron microscope. A total of eight neuropil fields from two P24 WT mice and eight neuropil fields from two P24 nNOS-KO mice, with total areas of 2,121 μm^2 and 2,185 μm^2, respectively, were analyzed using Neurolucida software. The total area of all dendritic profiles in a field was calculated and normalized to the total area of the respective field.

EE Experiments. P14 $nNOS^{-/-}$ pups and their WT littermates were exposed together with their mothers to EE conditions for 10 d. Pups were tattooed and genotyped in the first week after their birth. The EE consisted of a rat microisolator cage (much bigger size than regular mouse microisolator cage) with many different additional preliminary autoclaved objects inside the cage, such as running wheel, mouse igloo, and also plastic and paper tunnels, plastic laboratory grids, holders, tubes, lids, and so forth. The objects in the cage were changed daily. Control $nNOS^{-/-}$ and WT pups were raised with their mother under standard housing conditions for the same duration (P14–P24) After 10 d, all $nNOS^{-/-}$ and WT pups of control and EE groups were perfused with 2% PFA/3%GA in 0.1 M Phosphate buffer (pH 7.4), postfixed with the same solution overnight at 4 °C, and processed for electron microscopy.

Analysis of Spatial Arrangement of Synapses. The spatial distribution of synapses was analyzed in small sampling windows (8 × 6-μm area, six consecutive aligned sections, 0.36 μm of total thickness; total volume: 17.28 μm^3) using minimum spanning tree (MST) and radial distribution function (RDF) algorithms. MST is the shortest network of line segments that interconnects a set of given points without a closed path. MST analysis, carried out using custom written software, included all dots occurring within an individual sampling window. The RDF algorithm was integrated in custom software written in Delphi (v7, Borland Software) and was used to describe the probability of a neighbor-synapse to occur close to the reference one. Every spine synapse in the sampling window was marked with a dot in the middle of its PSD using Neurolucida software thus allowing to represent the spatial pattern of spine synapse distribution on a 2D plane. The coordinates of the dots were measured with UTHSCSA ImageTool software (v3, University of Texas, San Antonio, TX) using the point tool. One by one, all of the dots representing synapses in the central part of the sampling window were considered as reference ones. We measured the number of the dots that occurred within concentric annuli centered on the reference dot and defined by widths of 0.2 μm. The number of dots present in annuli at increasing distances from the reference dot was counted and normalized to the total number of dots in the sampling window. In total, a central circle and four annuli were analyzed representing a total area of 1 μm in radius corresponding to the estimated diffusion distance for NO. In RDF analysis, the dots found within 0.5-μm-wide edge zone all around the sampling window were not considered as reference dots to avoid edge effects. The same procedure was applied to the simulated uniform random distributions of 60 dots within sampling windows of the same size (n = 14 simulated distributions).

Statistical Analyses. All data are presented as mean ± SEM, and comparisons were made using a two-tailed Student t test, unless otherwise indicated.

SI Material. Fig. S1 shows the alterations of synaptic network development produced by chronic blockade of NO production in rat pups. Fig. S2 shows that loss of NO signaling did not affect the length and distribution of apical dendritic arbors. Fig. S3 shows the changes in excitatory transmission and intrinsic cell properties produced by L-NAME treatment. Fig. S4 provides evidence for activity-dependent VASP phosphorylation. Table S1 provides all quantitative values and statistical data related to the ultrastructural EM analyses of the effects of blocking NO production on synapse morphology. Table S2 provides all quantitative values and statistical data related to the spine dynamics analyses.

ACKNOWLEDGMENTS. We thank Marlis Moosmayer and Lorena Jourdain for excellent technical support; Fred Pillonel and Adrian Duran for the help with

the image alignment; David B. Pearse (Johns Hopkins Bayview Medical Center) for a generous gift of the vasodilator-stimulated phosphoprotein plasmid constructions; Joel Spaltenstein for the development of the Osirix software plugin; and Paul Klauser and Mathias De Roo for experimental help and advice. This work was supported by the Swiss National Science Foundation Grant 310030B-144080 and National Center of Competence in Research Synapsy (D.M.) and Grant 11.G34.31.0071 from Russian Ministry of Education and Science (to G.E.).

1. Holtmaat A, Wilbrecht L, Knott GW, Welker E, Svoboda K (2006) Experience-dependent and cell-type-specific spine growth in the neocortex. *Nature* 441 (7096):979–983.
2. Holtmaat A, De Paola V, Wilbrecht L, Knott GW (2008) Imaging of experience-dependent structural plasticity in the mouse neocortex in vivo. *Behav Brain Res* 192(1):20–25.
3. Yang G, Pan F, Gan WB (2009) Stably maintained dendritic spines are associated with lifelong memories. *Nature* 462(7275):920–924.
4. Xu T, et al. (2009) Rapid formation and selective stabilization of synapses for enduring motor memories. *Nature* 462(7275):915–919.
5. Hofer SB, Mrsic-Flogel TD, Bonhoeffer T, Hübener M (2009) Experience leaves a lasting structural trace in cortical circuits. *Nature* 457(7227):313–317.
6. Bednarek E, Caroni P (2011) β-Adducin is required for stable assembly of new synapses and improved memory upon environmental enrichment. *Neuron* 69(6):1132–1146.
7. Lai CS, Franke TF, Gan WB (2012) Opposite effects of fear conditioning and extinction on dendritic spine remodelling. *Nature* 483(7387):87–91.
8. Caroni P, Donato F, Muller D (2012) Structural plasticity upon learning: Regulation and functions. *Nat Rev Neurosci* 13(7):478–490.
9. De Roo M, Klauser P, Muller D (2008) LTP promotes a selective long-term stabilization and clustering of dendritic spines. *PLoS Biol* 6(9):e219.
10. Kleindienst T, Winnubst J, Roth-Alpermann C, Bonhoeffer T, Lohmann C (2011) Activity-dependent clustering of functional synaptic inputs on developing hippocampal dendrites. *Neuron* 72(6):1012–1024.
11. Fu M, Yu X, Lu J, Zuo Y (2012) Repetitive motor learning induces coordinated formation of clustered dendritic spines in vivo. *Nature* 483(7387):92–95.
12. Sattler R, et al. (1999) Specific coupling of NMDA receptor activation to nitric oxide neurotoxicity by PSD-95 protein. *Science* 284(5421):1845–1848.
13. Burette A, Zabel U, Weinberg RJ, Schmidt HH, Valtschanoff JG (2002) Synaptic localization of nitric oxide synthase and soluble guanylyl cyclase in the hippocampus. *J Neurosci* 22(20):8961–8970.
14. Christopherson KS, et al. (2003) Lipid- and protein-mediated multimerization of PSD-95: Implications for receptor clustering and assembly of synaptic protein networks. *J Cell Sci* 116(Pt 15):3213–3219.
15. Schuman EM, Madison DV (1991) A requirement for the intercellular messenger nitric oxide in long-term potentiation. *Science* 254(5037):1503–1506.
16. O'Dell TJ, Hawkins RD, Kandel ER, Arancio O (1991) Tests of the roles of two diffusible substances in long-term potentiation: Evidence for nitric oxide as a possible early retrograde messenger. *Proc Natl Acad Sci USA* 88(24):11285–11289.
17. Williams JH, et al. (1993) The suppression of long-term potentiation in rat hippocampus by inhibitors of nitric oxide synthase is temperature and age dependent. *Neuron* 11(5):877–884.
18. Cummings JA, Nicola SM, Malenka RC (1994) Induction in the rat hippocampus of long-term potentiation (LTP) and long-term depression (LTD) in the presence of a nitric oxide synthase inhibitor. *Neurosci Lett* 176(1):110–114.
19. Micheva KD, Buchanan J, Holz RW, Smith SJ (2003) Retrograde regulation of synaptic vesicle endocytosis and recycling. *Nat Neurosci* 6(9):925–932.
20. Nikonenko I, Jourdain P, Muller D (2003) Presynaptic remodeling contributes to activity-dependent synaptogenesis. *J Neurosci* 23(24):8498–8505.
21. Steinert JR, et al. (2008) Nitric oxide is a volume transmitter regulating postsynaptic excitability at a glutamatergic synapse. *Neuron* 60(4):642–656.
22. Garthwaite J (2008) Concepts of neural nitric oxide-mediated transmission. *Eur J Neurosci* 27(11):2783–2802.
23. Nugent FS, Penick EC, Kauer JA (2007) Opioids block long-term potentiation of inhibitory synapses. *Nature* 446(7139):1086–1090.
24. Kelley JB, Balda MA, Anderson KL, Itzhak Y (2009) Impairments in fear conditioning in mice lacking the nNOS gene. *Learn Mem* 16(6):371–378.
25. Wass C, Klamer D, Fejgin K, Pålsson E (2009) The importance of nitric oxide in social dysfunction. *Behav Brain Res* 200(1):113–116.
26. Tanda K, et al. (2009) Abnormal social behavior, hyperactivity, impaired remote spatial memory, and increased D1-mediated dopaminergic signaling in neuronal nitric oxide synthase knockout mice. *Mol Brain* 2:19.
27. Shinkai T, Ohmori O, Hori H, Nakamura J (2002) Allelic association of the neuronal nitric oxide synthase (NOS1) gene with schizophrenia. *Mol Psychiatry* 7(6):560–563.
28. Bernstein HG, Keilhoff G, Steiner J, Dobrowolny H, Bogerts B (2011) Nitric oxide and schizophrenia: Present knowledge and emerging concepts of therapy. *CNS Neurol Disord Drug Targets* 10(7):792–807.
29. Packer MA, et al. (2003) Nitric oxide negatively regulates mammalian adult neurogenesis. *Proc Natl Acad Sci USA* 100(16):9566–9571.
30. Kwiatkowski AV, et al. (2007) Ena/VASP Is Required for neuritogenesis in the developing cortex. *Neuron* 56(3):441–455.
31. Applewhite DA, et al. (2007) Ena/VASP proteins have an anti-capping independent function in filopodia formation. *Mol Biol Cell* 18(7):2579–2591.
32. Lin YL, Lei YT, Hong CJ, Hsueh YP (2007) Syndecan-2 induces filopodia and dendritic spine formation via the neurofibromin-PKA-Ena/VASP pathway. *J Cell Biol* 177(5): 829–841.
33. Lindsay SL, Ramsey S, Aitchison M, Renné T, Evans TJ (2007) Modulation of lamellipodial structure and dynamics by NO-dependent phosphorylation of VASP Ser239. *J Cell Sci* 120(Pt 17):3011–3021.
34. Rentsendorj O, et al. (2008) Role of vasodilator-stimulated phosphoprotein in cGMP-mediated protection of human pulmonary artery endothelial barrier function. *Am J Physiol Lung Cell Mol Physiol* 294(4):L686–L697.
35. Moser MB, Trommald M, Andersen P (1994) An increase in dendritic spine density on hippocampal CA1 pyramidal cells following spatial learning in adult rats suggests the formation of new synapses. *Proc Natl Acad Sci USA* 91(26):12673–12675.
36. Gogolla N, Galimberti I, Deguchi Y, Caroni P (2009) Wnt signaling mediates experience-related regulation of synapse numbers and mossy fiber connectivities in the adult hippocampus. *Neuron* 62(4):510–525.
37. Landers MS, Knott GW, Lipp HP, Poletaeva I, Welker E (2011) Synapse formation in adult barrel cortex following naturalistic environmental enrichment. *Neuroscience* 199:143–152.
38. Roberts TF, Tschida KA, Klein ME, Mooney R (2010) Rapid spine stabilization and synaptic enhancement at the onset of behavioural learning. *Nature* 463(7283): 948–952.
39. Keck T, et al. (2008) Massive restructuring of neuronal circuits during functional reorganization of adult visual cortex. *Nat Neurosci* 11(10):1162–1167.
40. Brenman JE, et al. (1996) Interaction of nitric oxide synthase with the postsynaptic density protein PSD-95 and alpha1-syntrophin mediated by PDZ domains. *Cell* 84(5): 757–767.
41. Garthwaite J, Charles SL, Chess-Williams R (1988) Endothelium-derived relaxing factor release on activation of NMDA receptors suggests role as intercellular messenger in the brain. *Nature* 336(6197):385–388.
42. Turrigiano GG, Leslie KR, Desai NS, Rutherford LC, Nelson SB (1998) Activity-dependent scaling of quantal amplitude in neocortical neurons. *Nature* 391 (6670):892–896.
43. Arnold WP, Mittal CK, Katsuki S, Murad F (1977) Nitric oxide activates guanylate cyclase and increases guanosine 3′:5′-cyclic monophosphate levels in various tissue preparations. *Proc Natl Acad Sci USA* 74(8):3203–3207.
44. Bartus K, Pigott B, Garthwaite J (2013) Cellular targets of nitric oxide in the hippocampus. *PLoS ONE* 8(2):e57292.
45. Wang HG, et al. (2005) Presynaptic and postsynaptic roles of NO, cGK, and RhoA in long-lasting potentiation and aggregation of synaptic proteins. *Neuron* 45(3): 389–403.
46. Richards DA, et al. (2005) Glutamate induces the rapid formation of spine head protrusions in hippocampal slice cultures. *Proc Natl Acad Sci USA* 102(17):6166–6171.
47. Kwon HB, Sabatini BL (2011) Glutamate induces de novo growth of functional spines in developing cortex. *Nature* 474(7349):100–104.
48. Dubos A, et al. (2012) Alteration of synaptic network dynamics by the intellectual disability protein PAK3. *J Neurosci* 32(2):519–527.
49. Nikonenko I, et al. (2008) PSD-95 promotes synaptogenesis and multiinnervated spine formation through nitric oxide signaling. *J Cell Biol* 183(6):1115–1127.
50. Rose EJ, et al. (2012) The NOS1 variant rs6490121 is associated with variation in prefrontal function and grey matter density in healthy individuals. *Neuroimage* 60(1): 614–622.
51. Stoppini L, Buchs PA, Muller D (1991) A simple method for organotypic cultures of nervous tissue. *J Neurosci Methods* 37(2):173–182.
52. Sterio DC (1984) The unbiased estimation of number and sizes of arbitrary particles using the disector. *J Microsc* 134(Pt 2):127–136.